

We are IntechOpen, the world's leading publisher of Open Access books Built by scientists, for scientists

6,900

Open access books available

186,000

International authors and editors

200M

Downloads

Our authors are among the

154

Countries delivered to

TOP 1%

most cited scientists

12.2%

Contributors from top 500 universities



WEB OF SCIENCE™

Selection of our books indexed in the Book Citation Index
in Web of Science™ Core Collection (BKCI)

Interested in publishing with us?
Contact book.department@intechopen.com

Numbers displayed above are based on latest data collected.
For more information visit www.intechopen.com



Synthesis of Cobalt-Based Nanomaterials from Organic Precursors

Maria Smyrnioti and Theophilos Ioannides

Additional information is available at the end of the chapter

<http://dx.doi.org/10.5772/intechopen.70947>

Abstract

Development of efficient and low-cost methods for the production of cobalt and cobalt oxide nanoparticles is of great interest. Such nanoparticles are typically prepared via transformation of precursors under controlled conditions. In the case of organic precursors, the production of said nanoparticles takes place through thermal decomposition of the organic moiety. The decomposition pathway of the precursor is greatly dependent on the type (i.e. inert, reducing or oxidizing) of the gaseous atmosphere prevailing during heating, as well as on the heating schedule itself. The characteristics of the organic group have also an important influence on the structure of the final material. The goal of the current work is to present a comprehensive review of the research work focusing on the synthesis of cobalt-based nanomaterials from activation of organic precursors.

Keywords: pyrolysis, carboxylates, thermal treatment, cobalt oxides, cobalt, Co_3O_4 , nanoparticles, nanomaterials

1. Introduction

Nanostructured materials exhibit novel properties, which notably differ from those of the corresponding bulk solid, due to the small size effect [1]. Transition metal-oxide nanoparticles have attracted considerable interest on account of their applications in various fields, including catalysis, electronics, coatings, gas sensing, electrochemical devices, solar energy conversion and biomedicine [2, 3]. Several methods have been employed for the synthesis of cobalt nanomaterials, including: (i) microemulsion, (ii) solvothermal method, (iii) thermal decomposition of cobalt precursors, (iv) spray pyrolysis, (v) sol-gel process, etc. [1, 4, 5]. Thermal decomposition is a commonly employed method for preparation of nanoscale cobalt or cobalt

oxide, due to process simplicity, short reaction time, and, most importantly, low-cost and efficiency. Such nanoparticles are typically prepared via transformation of precursors under controlled conditions. There are many potential precursors, such as, inorganic and organic salts and metal-organic frameworks (MOFs). The decomposition pathway of the precursor depends on the type of the gaseous atmosphere prevailing during heating, on the heating schedule itself, as well as on the characteristics of the organic group. Co-addition of other metal cations toward a mixed metal-organic precursor provides a straightforward approach to the synthesis of mixed metal oxides. Additionally, supported cobalt-based nanomaterials (i.e. cobalt oxide/graphene composites) can be fabricated. The aim of the current work is to present a comprehensive review of the research focusing on synthesis of cobalt-based nanomaterials from activation of organic precursors.

2. Cobalt and cobalt oxide nanoparticles from carboxylates

A major group of organic precursors that have been employed for the synthesis of cobalt and cobalt oxide nanoparticles via a thermal decomposition route is cobalt-carboxylate salts. The “carboxylate” term includes several organic species that contain at least one carboxyl group, such as oxalate, citrate, etc. Methods for synthesis of cobalt-carboxylates include (i) sol-gel [2, 4], (ii) intimate mixing of cobalt ions [6–8], (iii) precipitation [9, 10], (iv) hot oxidation-redox reaction [11], (v) ball milling [12] and (vi) microemulsion [13]. Reaction of cobalt acetate with a carboxylic acid, for example, leads directly to the synthesis of cobalt-carboxylate, when the carboxylic acid in question is stronger than acetic acid: $\text{Co}(\text{Ac})_2 + \text{RCOOH} \rightarrow \text{Co}(\text{RCOO})_2 + 2 \text{AcH}$ (1). This cannot be the case when cobalt nitrate or cobalt chloride is employed, since nitrate and chloride anions are weak conjugate bases of the strong nitric and hydrochloric acids. Nevertheless, many research groups choose to utilize metal-inorganic salts to synthesize cobalt-carboxylate precursors. Thermal treatment of the synthesized carboxylate precursor leads to the removal of the organic species, thus cobalt or cobalt oxide nanoparticles are formed. In the following sections, a review of the synthetic protocols for synthesis of cobalt-based nanomaterials from cobalt-carboxylates is presented.

2.1. Cobalt oxide nanoparticles from oxalate precursors

There are several publications concerning the synthesis of cobalt or cobalt oxide nanoparticles from oxalate precursors. Abdelkader et al. synthesized Co_3O_4 nanoparticles by calcination of cobalt (II) oxalate dihydrate in static air at 500°C for 2 h [14]. Thota et al. employed a sol-gel process to synthesize oxalate precursors and their subsequent thermal treatment to produce Co_3O_4 nanocrystallites. More specifically, cobalt acetate tetrahydrate was dissolved in ethanol at $35\text{--}40^\circ\text{C}$ under continuous stirring followed by oxalic acid addition to yield a thick gel. Thermal decomposition of the dried gel in air at $400\text{--}600^\circ\text{C}$ for 2 h led to Co_3O_4 [4]. Luisetto et al. have also produced Co_3O_4 by thermal treatment of cobalt oxalate precipitate at 450°C for 2 h in air [2]. de Rivas et al. prepared Co_3O_4 nanoparticles via

calcination of oxalate nanorods at 500°C in static air [15]. Cobalt oxalate precursors have been also prepared from cobalt nitrate, cobalt chloride or cobaltous hydroxide carbonate. Shen et al. obtained CoO nanoparticles from the decomposition of corresponding oxalates at 500°C for 4 h in air. Oxalates were prepared via precipitation from a solution of cobalt nitrate, oxalic acid and ethanol [16]. Manteghi et al. synthesized Co₃O₄ nanostructures by thermal decomposition of cobalt oxalate synthesized by precipitation from cobalt nitrate or cobalt chloride and ammonium oxalate in the presence or absence of surfactants [17]. Yuan et al. synthesized Co₃O₄ by annealing cobalt oxalate precursors prepared via hydrothermal and rheological phase reaction methods [18, 19].

2.2. Cobalt oxide nanoparticles from citrate precursors

Manouchehri et al. reported on the synthesis of Co₃O₄ and CoO nanoparticles via solid state ball milling of cobalt acetate and citric acid powders and subsequent calcination of the prepared carboxylate precursors [12]. de Rivas et al. also used ball milling for synthesis of cobalt citrate starting from cobalt carbonate and citric acid [20]. An aqueous sol-gel citrate procedure has been employed by many research groups initiating from cobalt nitrate and citric acid and the obtained precursors were thermally decomposed between 300 and 500°C in static air for 4 h [20–22]. Pudukudy et al. chose a simple solid-state mixing of cobalt nitrate with various modifiers such as citric acid, glucose, sucrose and urea. The components were mixed, pulverized and heated at 80°C for 1 h. The bimodal mesoporous spinel cobalt oxide nanomaterials were prepared by calcination at 300°C for 2 h [23].

2.3. Cobalt and cobalt oxide nanoparticles from malonate precursors

Mohamed et al. synthesized cobalt malonates by precipitation using cobalt chloride and disodium malonate or malonic acid. The precipitates were heated up to 500°C at heating rates between 2 and 20°C min⁻¹ in a dynamic atmosphere of N₂, H₂ or air resulting in cobalt oxides and metallic cobalt [10]. Stefanescu et al. synthesized nanosized cobalt oxides unsupported [3] or dispersed in a SiO₂ matrix [24] by thermal decomposition of compounds resulting from a redox reaction of cobalt nitrate and diols (1,2-ethanediol, 1,3-propanediol). The produced carboxylates were oxalate, glyoxylate and malonate. The redox reaction between the NO₃⁻ ions and -OH groups of each diol took place under controlled heating (90–120°C, 2 h) and the resulting powders were annealed at 350 and 1000°C for 3 h in ambient air.

2.4. Cobalt and cobalt oxide nanoparticles from succinate precursors

Ganguly et al. synthesized cobalt and cobalt oxide nanoparticles from cobalt succinate originated from a reverse micellar method using cobalt nitrate, 1-butanol and CTAB (as the surfactant). The collected product by centrifugation was thermally decomposed under N₂ at 650°C and under air at 500°C for 6 h, yielding pure Co and Co₃O₄, respectively [13].

2.5. Cobalt oxide nanoparticles from tartrate precursors

Bhattacharjee et al. reported the synthesis of Co_3O_4 nanoparticles by thermal decomposition at 400–600°C of cobalt (II)-tartrate complex prepared by a modified sol-gel route employing cobalt nitrate and tartaric acid [25]. Palacios-Hernández et al. prepared CoO and Co_3O_4 nanoparticles by thermal treatment of cobalt tartrate synthesized by precipitation. Cobalt tartrate was obtained by mixing solutions of cobalt nitrate and the disodium salt of L-tartaric acid. The nanoparticles were prepared by thermal decomposition of the metal-organic complex under isothermal conditions at 500°C in the presence of air for 4 h [26].

2.6. Cobalt oxide nanoparticles from other carboxylate precursors

Chen et al. synthesized CoO nanoparticles using cobalt oleate as precursor. Cobalt chloride and sodium oleate were used as initial chemicals and the obtained dried precipitate was dissolved with oleic acid in 1-octadecene. The CoO nanoparticles were produced by heating the mixture up to 320°C and maintaining that temperature for 30 min [27]. Assim et al. presented the synthesis of a series of ethylene glycol-functionalized cobalt (II) carboxylates by an anion exchange reaction of cobalt (II) acetate tetrahydrate with the corresponding acids. Co_3O_4 nanoparticles were prepared by solid state thermal decomposition of $\text{Co}(\text{CO}_2\text{CH}_2(\text{OC}_2\text{H}_4)_2\text{OMe})_2$ at 300°C, while different decomposition times of 10, 20 and 30 min were applied [28]. Semenov et al. prepared cobalt composites via thermal treatment under isothermal conditions (335°C for 9 h under Ar) of unsaturated cobalt dicarboxylates (hydrogen allylmalonate, acetylenedicarboxylate, itaconate, maleate, glutaconate, cis-muconate) using cobalt carbonate and an unsaturated dicarboxylic acid aqueous solution [9].

3. Mixed metal-oxide nanoparticles from carboxylate precursors

Mixed metal oxides contain two or more metallic ions in proportions that may either be defined by stoichiometry or variable. One way to classify mixed metal oxides is according to their crystalline structure (spinel, perovskites, etc.) [29].

3.1. Spinel mixed metal-oxide nanoparticles from carboxylate precursors

The preparation methods for CoFe_2O_4 nanoparticles require specialized techniques to prevent agglomeration. Diodati et al. synthesized various spinel ferrites (CoFe_2O_4 , NiFe_2O_4 , ZnFe_2O_4 and MgFe_2O_4) by a wet-synthesis coprecipitation route starting from iron(III) nitrate, cobalt(II) chloride and oxalic acid in order to prepare the oxalate precursors. The precipitate was centrifuged, dried and calcined at 873 or 1173 K for 5 h in air [30]. Many researchers used the redox method to synthesize the carboxylate precursors (oxalate, malonate, succinate, etc.) initiating from iron(III) nitrate, cobalt(II) nitrate and various diols (ethylene glycol, 1,2-propanediol, 1,3-propanediol and 1,4-butanediol). The obtained precursors were calcined at various temperatures in air to cobalt ferrites [11, 31, 32]. In some cases, the synthesized ferrites were

dispersed in a SiO₂ matrix using a modified sol-gel and redox reaction method [31, 33–35]. Amiri et al. synthesized CoFe₂O₄/SiO₂ nanocomposites by a procedure described as sol-gel autocombustion method. Iron and cobalt nitrate were dissolved in water and acid solutions (maleic, malonic, trimesic and ascorbic acid) were added separately as well as tetraethoxysilane. The sols were transformed into gel at 40°C for 24 h [36]. Cobalt-zinc ferrite, Co_{1-x}Zn_xFe₂O₄ (x varying from 0 to 1) was obtained by thermal decomposition of the carboxylate precursor, starting from a mixture of Fe(III), Co(II) and Zn(II) nitrates and 1,3-propanediol whereas a redox reaction took place. The precursor was decomposed at 300°C and further annealed in air for 3 h at various temperatures from 350 to 1000°C [37, 38].

Mixed cobalt-manganese oxide is another spinel synthesized by thermal decomposition of carboxylate salts. Papadopoulou et al. obtained Co-MnO catalysts from the pyrolytic decomposition of mixed cobalt-manganese fumarate and gluconate salts. The precursor compounds were prepared by mixing aqueous solution of cobalt and manganese acetate with an aqueous solution of D-gluconic acid or an ethanolic solution of fumaric acid. The corresponding mixed metal/metal-oxide nanoparticles were prepared by thermal decomposition of the organic precursors under inert gas flow in the temperature range of 500–700°C. Cobalt-manganese spinel oxide was also prepared via oxidative treatment of the same mixed carboxylates at 500°C for 2 h [6–8]. Faure et al. prepared Co_xMn_{3-x}O₄ (0 ≤ x ≤ 3) by controlled decomposition of mixed oxalates, precipitated at room temperature using cobalt nitrate, manganese nitrate and ammonium oxalate. The thermal decomposition of oxalates was carried out near 200°C under O₂/Ar flow and further calcination up to 300°C for 1 h [39].

Wang et al. synthesized CoAl₂O₄ nanoparticles via thermal treatment of Co-Al-glycine precursors, initiating from cobalt and aluminum nitrate and glycine. The precursor was treated under air at 200–1000°C for 2 h [40]. Synthesis of CoCr₂O₄, a member of the chromite spinel family, was reported by Gingasu et al. via thermal decomposition of tartrate and gluconate precursors obtained by precipitation using cobalt (II) nitrate, chromium (III) nitrate and tartaric acid or δ-gluconolactone [41]. Finally, synthesis of metal cobaltite spinels (MgCo₂O₄, NiCo₂O₄) by thermal decomposition of coprecipitated mixed oxalate precursors has been reported [42, 43].

3.2. Perovskite mixed metal nanoparticles from carboxylate precursors

Seyfi et al. synthesized unsupported perovskite samples (i.e. LaCoO₃) by thermal decomposition of citrate complexes using lanthanum(III) nitrate, cobalt(II) nitrate and citric acid as initial compounds. The obtained viscous gel was dried and calcined at 700°C for 5 h under air atmosphere [44].

3.3. Ilmenite mixed metal-oxide nanoparticles from carboxylate precursors

Gabal et al. prepared CoTiO₃ via a coprecipitation method. The mixed oxalate precursor was thermally treated at various temperatures (230–950°C, 30 min and 1000°C, 2 h) and CoTiO₃ nanoparticles were obtained [45].

4. Supported cobalt oxide from carboxylate salts

Transition metal oxides have been proposed as materials for lithium-ion batteries (LIBs) and it has been reported that the performance of cobalt oxides is further improved if cobalt oxide nanoparticles are supported on carbon (nanofibers, nanoflakes, etc.) [46]. From this point of view, Guo et al. synthesized Co_3O_4 /graphite composites by precipitation of cobalt oxalate on the surface of graphite and pyrolysis of the precipitate [47].

5. Cobalt-based nanomaterials from metal-organic frameworks (MOFs)

A number of recent publications have reported on the synthesis of cobalt-based nanomaterials embedded in carbon, employing metal-organic framework compounds as precursors. Metal-organic frameworks (MOFs) are an emerging class of porous materials constructed from metal-containing nodes and organic linkers [46]. Wang et al. showed that the direct pyrolysis of cobalt nitrate accommodated by impregnation in the pores of ZIF-8 and ZIF-67 yields Co_3O_4 nanoparticles [48]. Ashouri et al. utilized the thermal decomposition of cobalt-terephthalate MOF precursor as a synthetic route for the fabrication of Co_3O_4 nanoparticles [49]. Pei et al. synthesized carbon-supported and Si-doped carbon-supported Co nanomaterials by the thermolysis of Co-MOF-71 at 600°C for 8 h under He flow [50]. Many researchers have utilized MOFs as precursors for the synthesis of cobalt-based nanoparticles embedded in carbon. Zhou et al. prepared nitrogen-doped carbon-embedded Co catalysts by one-step pyrolysis (600–900°C, for 8 h, under N_2) of ZIF-67 with silica as the hard template [51] while, Khan et al. used direct carbonization of ZIF-12 at 950°C for 6 h under Ar atmosphere [52]. Lu et al. fabricated metallic Co nanoparticles embedded in N-doped porous carbon layers by thermal treatment of macroscale Co-MOFs obtained by using 1,3,5-benzenetricarboxylic acid, triethylamine and nonanoic acid, at various temperatures (800, 900, 1000°C) for 1 h under N_2 atmosphere [53]. Qiu et al. obtained cobalt-based nanoparticles coated with a thin carbon shell from Co-MOF-74 via a two-step carbonization where at first the cobalt precursor was heated at 700°C for 2 h under Ar atmosphere to produce cobalt nanoparticles coated with carbon shell and in a second phase the as-synthesized material was calcined either at 500°C for 1 h under CO_2 atmosphere to produce carbon-coated Co_3O_4 nanoparticles or for 30 min under the same conditions to produce Co/CoO nanomaterials. Pure Co_3O_4 nanocrystals were obtained by treating carbon-coated cobalt nanoparticles at 250°C for 2 h under air atmosphere [54].

6. Structure and characterization of cobalt-based nanoparticles

6.1. Structure and characterization of Co_3O_4 nanoparticles

The majority of publications for the synthesis of cobalt-based nanoparticles from thermal decomposition of organic precursors under air have reported on the formation of the spinel

Co_3O_4 phase. The published X-Ray Diffraction (XRD) patterns have reflection peaks that can be perfectly indexed to the cubic phase of Co_3O_4 spinel with the cell parameter a in the range 8.07–8.15 Å and space group $\text{Fd}3\text{m}$ (**Figure 1**). In most cases, there were no diffraction peaks related to CoO or metallic cobalt (Co^0), except for thermal treatment above 900°C, where Co_3O_4 decomposes to CoO . The average crystallite size, estimated by the Debye-Scherrer equation, varied between 5 and 50 nm, depending on the preparation method and the type of cobalt precursor, the thermal treatment conditions, etc. Structural details of Co_3O_4 have been investigated by Scanning Electron Microscopy (SEM) and Transmission Electron Microscopy (TEM). SEM results indicated the agglomeration of Co_3O_4 nanoparticles and various types of morphologies were observed, that is, matchstick type bars [4, 17], nanorods of bamboo stick type [4], truncated hexahedral shape [18], flocculent-like structures [48] and irregularly shaped aggregates (dense clusters) [21, 22, 26, 49]. TEM results were relatively consistent with XRD results concerning the crystallite size (5–50 nm). Palacios-Hernández et al. reported the synthesis of Co_3O_4 with average grain size of 300 nm and a scarce number of nanoparticles with a diameter of 100 nm and smaller, according to TEM. Most nanoparticles had faceted morphology and high crystalline quality as verified by Selected-Area Electron Diffraction (SAED) analysis and High-Resolution Transmission Electron Microscopy (HRTEM) [26]. Pseudo-hexagonal [15, 17, 18, 21], circular and occasionally rectangular [2] or uniform spherical [12] shaped nanoparticles were observed. In general, powders are homogeneously dispersed with dimensions ranging from 50 to 600 nm, in accordance with SEM results, mentioned above. TEM images further validated that the porous architectures—agglomerations—are constructed from the interconnection among the primary crystalline nanoparticles with size of a few nanometers. Furthermore, the regular diffraction spots displayed from SAED pattern, validated the cubic face-centered structure of Co_3O_4 [2, 4, 18, 25]. HRTEM analysis also indicated the single crystalline nature of Co_3O_4 [18, 25].

The textural properties of cobalt oxides are typically determined by N_2 adsorption-desorption at liquid N_2 temperature. The reported Brunauer–Emmett–Teller (BET) specific surface area and Barrett-Joyner-Halenda (BJH) pore size distribution of Co_3O_4 nanoparticles

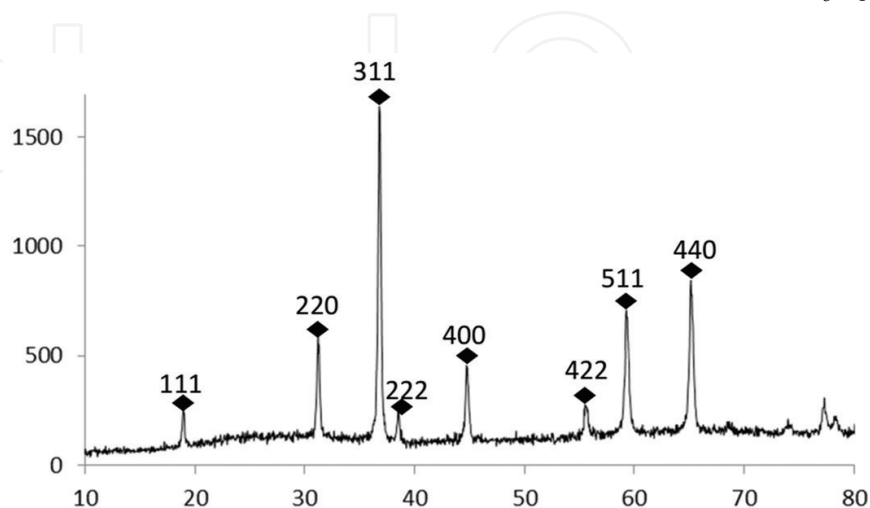


Figure 1. Typical XRD pattern of pure Co_3O_4 [17].

differ significantly from sample to sample. Factors like the synthesis method of cobalt precursor, its nature, the treatment temperature and soak time affect their textural properties. The specific surface areas of Co_3O_4 nanoparticles vary from 7 [23] to $120 \text{ m}^2 \text{ g}^{-1}$ [21], the pore volume ranges between 0.03 [23] and $0.24 \text{ cm}^3 \text{ g}^{-1}$ [20] while average pore size is between 9 [20] and 68 nm [23]. Wang et al. found that all N_2 sorption isotherms of Co_3O_4 and Co-Ce oxide nanoparticles can be assigned to a type IV isotherm, typical for mesoporous materials, showing a hysteresis loop at $P/P_0 = 0.45$ [22]. The mesoporous structure of the nanomaterials was also noted by other researchers [15, 17, 20, 23]. Pudukudy et al. synthesized Co_3O_4 spinels possessing a bimodal mesopore distribution in the presence of modifiers [23]. Manteghi et al. also suggested the presence of a secondary porous structure formed by aggregation of primary nanostructures [17]. Another very useful technique for the characterization of cobalt oxide and its precursors is Fourier Transform Infrared spectroscopy (FTIR) spectroscopy. The appearance of characteristic infrared absorption bands of cobalt precursor and final product obtained from thermal decomposition of the precursor validates their formation. The IR spectrum of cobalt oxide exhibits two major bands at $\sim 570 \text{ cm}^{-1}$ (ν_1) and $\sim 670 \text{ cm}^{-1}$ (ν_2) (**Figure 2a**). The first band (ν_1) is associated with the Co^{3+} vibration in the octahedral hole and the second band (ν_2) is attributed to the Co^{2+} vibration in the tetrahedral hole, which confirms the formation of the Co_3O_4 spinel [12, 17, 23, 24, 48, 49]. Raman spectroscopy has also been utilized for the confirmation of Co_3O_4 formation. Typically, five Raman bands at 198, 484, 522, 622 and 694 cm^{-1} are visible in the range $100\text{--}800 \text{ cm}^{-1}$, which correspond, respectively, to the F_{2g}^1 , E_g , F_{2g}^2 , F_{2g}^3 and A_{1g} modes of crystalline Co_3O_4 (**Figure 2b**). F_{2g} and E_g modes are associated with the vibration of tetrahedral and octahedral sites, whereas the high-frequency band, A_{1g} mode, is linked to the occurrence of octahedral sites [14, 15, 20–22, 25].

The surface chemical status and composition of the nanomaterials can be investigated by means of X-ray photoelectron spectroscopy (XPS). According to XPS results, the Co_{2p} spectrum is decomposed into two distinct peaks and two weak satellites (**Figure 3a**). The two spin orbit

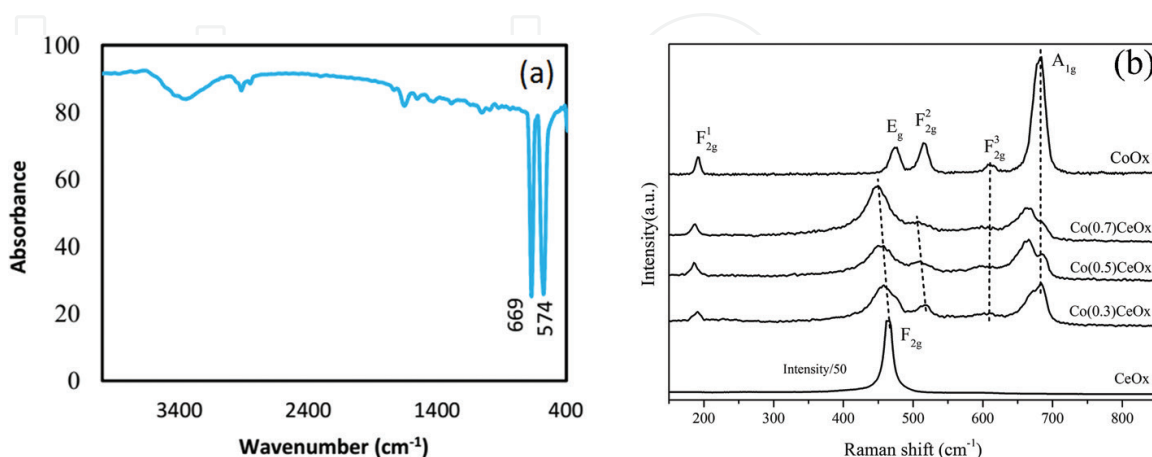


Figure 2. Typical (a) FTIR [17] and (b) Raman [22] spectra of Co_3O_4 nanostructures.

doublets assigned to cobalt oxides located at 780.8 and 795.9 eV can correspond to $\text{Co}_{2p(3/2)}$ and $\text{Co}_{2p(1/2)}$, respectively. The spin orbit doublet of $\text{Co}_{2p(3/2)}$ can be deconvoluted into two peaks at 780.8 and 782.3 eV, which are attributed to $\text{Co}^{3+}_{2p(3/2)}$ and $\text{Co}^{2+}_{2p(3/2)}$ configurations, respectively. The $\text{Co}_{2p(1/2)}$ spin orbit doublet can also be deconvoluted into two distinct peaks located at binding energies of 795.8 and 797.4 eV and are assigned to $\text{Co}^{3+}_{2p(1/2)}$ and $\text{Co}^{2+}_{2p(1/2)}$, respectively. The energy difference of 15.1 eV between $\text{Co}_{2p(3/2)}$ and $\text{Co}_{2p(1/2)}$ splitting is characteristic of the Co_3O_4 cubic phase. The presence of the two satellite peaks ($\text{Co}_{\text{sat.}}$) in the vicinity of the two spin orbit doublets, at binding energies of 788.2 and 804.8 eV, further demonstrates the existence of cobalt oxides [22, 55]. The XPS spectrum of O_{1s} presented in **Figure 3b** demonstrates a peak at 530.0 eV attributed to lattice oxygen of Co_3O_4 ($\text{O}_{\text{latt.}}, \text{O}^{2-}$) and another one at 531.0 eV associated with adsorbed oxygen onto surface oxygen vacancies and oxygen-containing groups such as hydroxyl species. The additional peak at 532.1 eV can be attributed to physical and chemical adsorption of water on the surface of defects ($\text{O}_{\text{adsorbates}}$) and apparently is not always present in O_{1s} spectra [22, 55].

Reducibility and acidity-basicity are important properties affecting material behavior in a specific application. Temperature programmed reduction (TPR) of Co_3O_4 nanoparticles shows two main peaks. The first peak is located at 250–360°C and is assigned to reduction of Co^{3+} to Co^{2+} with the concomitant phase change to CoO and the second peak appears at 350–473°C corresponding to reduction of Co^{2+} to Co^0 . Peak temperature deviations in TPR might be due to structural variations of Co_3O_4 nanoparticles (particle size and faceting) and TPR protocols [2, 14, 20–22]. The acidic properties of Co_3O_4 nanoparticles have been studied by NH_3 -TPD. Abdelkader et al. performed NH_3 -TPD on Co_3O_4 pre-reduced at 400°C for 1 h and reported that the TPD profile contained two peaks, at 104 and 240°C, indicating the presence of two acidic sites [14]. de Rivas et al. carried out NH_3 -TPD experiments on Co_3O_4 nanomaterials pretreated in a O_2/He stream at 500°C and observed two ammonia desorption peaks at 190–200°C and 300–305°C as well as a shoulder at 250°C. They concluded that the peak at low

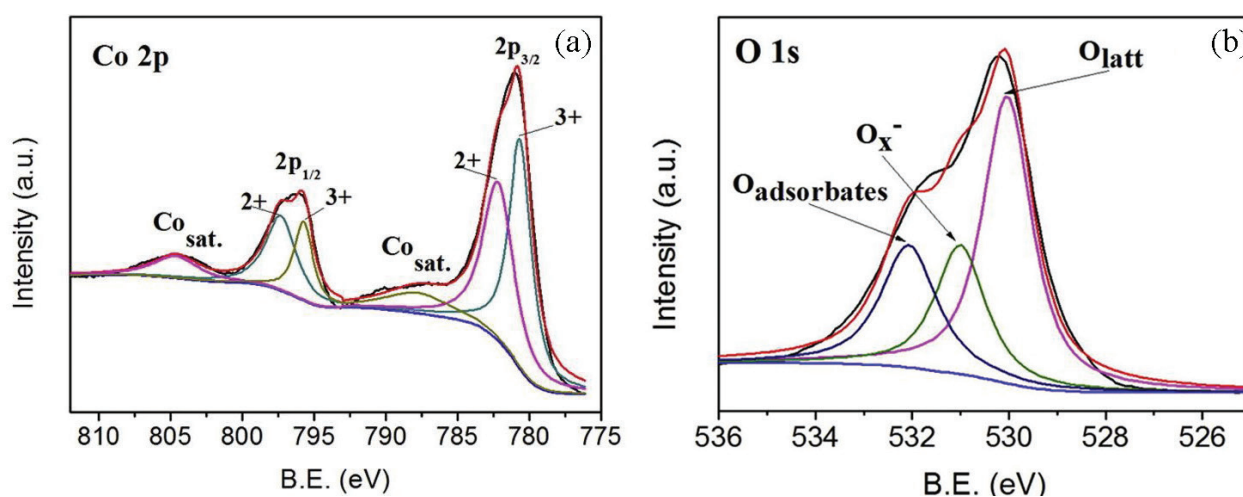


Figure 3. XPS spectra of (a) Co_{2p} region and (b) O_{1s} region [55].

temperature could be associated with weak acidic sites and the peak at high temperature with strong acidic sites [20]. In addition to physicochemical characterization of cobalt nanoparticles, some researchers have studied the optical, electrical and magnetic characteristics of the synthesized nanomaterials by means of UV-Vis-NIR Spectrometry [4], SQUID [4], cyclic voltammetry (CV) [17, 18] and electrochemical impedance spectroscopy (EIS) [17].

6.2. Structure and characterization of CoO nanoparticles

As already mentioned above, there is scarce bibliography concerning the preparation of CoO nanoparticles by thermal decomposition of cobalt-organic precursors. XRD results reported by Bartůněk et al. [5] and Manouchehri et al. [12] showed the presence of a face-centered cubic phase with cell parameter $a = 4.26 \text{ \AA}$ and space group F_33m [12]. In the FTIR spectrum, the appearance of a broad band at 450 cm^{-1} verified the formation of cubic CoO. According to TEM the as-prepared CoO consisted of two types of structures, small nanoparticles and nanorods [12]. Shen et al. claimed that the CoO nanoparticles exhibited quasi-spherical shape and their measured—from TEM micrographs—average particle size was 18 nm [16]. Chen et al. reported on flower-like CoO nanoparticles with an average particle size of 50 nm [27]. In some cases, synthesis of Co_3O_4 nanoparticles was accompanied by the formation of CoO or metallic cobalt as impurities. Pursuant to XRD results face-centered cubic (space group: F_33m) [23], monoclinic (space group: $C2/m$) [23] and tetragonal [9] crystal systems were reported.

6.3. Structure and characterization of metallic Co nanoparticles

Ganguly et al. produced pure metallic Co nanoparticles confirmed by XRD results with average size, as measured by TEM, between 10 and 40 nm [13]. Co composites were also synthesized by Semenov et al. containing, according to XRD data, metallic Co (hexagonal symmetry, unit cell parameters: $a = 2.506 \text{ \AA}$, $c = 4.071 \text{ \AA}$) and CoO as admixtures in the main phase of Co_3O_4 [9].

6.4. Structure and characterization of mixed metal-oxide nanoparticles

Dippong et al. synthesized CoFe_2O_4 nanoparticles and concluded that single phase cubic spinel CoFe_2O_4 can be produced at all temperatures initiating from 1,3-propanediol whereas, when initiating from 1,2-ethanediol and 1,2-propanediol elevated temperatures are required. The degree of CoFe_2O_4 crystallization increased with the increase of calcination temperature. The appearance of the intense, symmetric band at $560\text{--}585 \text{ cm}^{-1}$ in the FTIR spectra, characteristic of the CoFe_2O_4 phase, confirmed its formation, while, TEM results revealed—in accordance with XRD—the presence of CoFe_2O_4 as nearly spherical nanoparticles with dimensions varying with calcination temperature between 8 and 20 nm [11]. Another publication from the same group focused on the influence of Co/Fe ratio on the oxide phases in CoFe_2O_4 nanoparticles and proved the dependence of nanoparticle size on sample composition (Fe and Co content) and calcination temperature. The diameter

of the as-synthesized nanoparticles ranged between 12 and 88 nm and according to TEM micrographs, the spherical nanocrystallites showed an agglomerated conformation [56]. Similar work has been conducted by Stefanescu et al., who concluded that the average particle size of the nanoparticles estimated from XRD varied in the range 10–19 nm [32]. Diodati et al. synthesized CoFe_2O_4 and carried out in-situ temperature-dependent XRD of the oxalate precursors and showed that the XRD patterns of the spinel phase began to be visible at 773–873 K whereas they became sharp and distinct at 1073–1173 K. The crystallite size calculated by means of XRD and TEM was 23 nm (calcination at 873 K) and 185 nm (calcination at 1173 K). Furthermore, TEM micrographs showed that cobalt ferrite nanoparticles retained their identity and size but they had a tendency to form agglomerates. According to XPS and Mössbauer results, the as-synthesized compounds contained surface iron in oxidation state (III) and not in (II). The TPR result showed that the reduction process took place at 700–1173 K and resulted in the reduction of Co(II) and Fe(III) cations to a metallic state [30]. In addition, some researchers have studied the synthesis of CoFe_2O_4 embedded in SiO_2 and according to XRD results the formation of CoFe_2O_4 spinel phase is affected by various factors, that is, annealing temperature, percentage of silica matrix, the precursor type, etc. For instance, Dippong et al. have shown that the nanocrystallite size and crystallinity increased with increase of CoFe_2O_4 and decrease of SiO_2 content [34], with the use of longer chain precursors [31] and the increase of the annealing temperature [36]. The diameter of CoFe_2O_4 nanoparticles, calculated by means of XRD and TEM, ranged between 8 and 32 nm depending on the parameters mentioned above and according to SEM images they were spherical and formed irregular agglomerations [31, 34, 35]. Amiri et al. synthesized CoFe_2O_4 nanoparticles dispersed in a SiO_2 matrix by thermal decomposition of iron-cobalt-carboxylates (maleate, malonate, trimesate and ascorbate) and according to XRD patterns, the thermal decomposition of iron-cobalt trimesate precursor led to the formation of pure cubic spinel CoFe_2O_4 with a crystallite size of 7 nm. The formation of the CoFe_2O_4 phase was also confirmed by FTIR spectra due to the appearance of the characteristic bands at 469 and 694 cm^{-1} . FE-SEM analysis showed irregularly shaped nanoparticles with an average size of 36 nm (Fe-Co-malonate), 38 nm (Fe-Co-ascorbate) and 27 nm spherical nanoparticles with (Fe-Co-trimesate) and 37 nm (Fe-Co-maleate). All nanoparticles formed agglomerations according to SEM images [36]. Another nanomaterial prepared using thermal decomposition of the corresponding carboxylate precursors was $\text{Co}_{1-x}\text{Zn}_x\text{Fe}_2\text{O}_4$. Muntean et al. concluded by means of XRD that the as-synthesized nanomaterials consisted of the cubic spinel phase $\text{Co}_{1-x}\text{Zn}_x\text{Fe}_2\text{O}_4$ and impurities (CoFe_2O_4 , ZnFe_2O_4) except for the thermal decomposition at 1000°C, where $\text{Co}_{0.5}\text{Zn}_{0.5}\text{Fe}_2\text{O}_4$ ferrite was obtained as a single, well crystallized phase. The increase in annealing temperature increased the crystallinity and the crystallite size of the nanoparticles. The formation of mixed spinel structure was also confirmed by FTIR spectra due to the presence of characteristic bands at 400 and 600 cm^{-1} which indicate the anion-cation interaction in octahedral and tetrahedral voids. The average crystallite size varied between 11 and 81 nm depending on the annealing temperature [37]. Similar experiments performed by Stefanescu et al. led to particles with average crystallite size in the range 7–33 nm due to the lower annealing temperature (up to 600°C instead of 1000°C in Ref. [37]) [38].

Mixed cobalt-manganese oxides were investigated by Papadopoulou et al. [6–8]. They employed in-situ XRD to identify the evolving crystalline phases at various stages of pyrolysis of cobalt-manganese gluconate or fumarate precursors and concluded the formation of MnO and metallic Co phases at 550°C due to the thermal decomposition of the fumarate precursor, whereas the decomposition of gluconate precursor above 200°C did not lead to the formation of crystalline phases before 650°C. Same results were obtained by XRD measurements over passivated samples originated from fumarate salts. Thus, the thermal decomposition of both fumarate and gluconate precursors led to the formation of reduced Co-MnO phases in a single step, due to a carbothermal reaction that took place between residual carbon and Co^{2+} ions. Additionally, the specific surface area of all samples obtained from fumarate precursor ranged between 200 and 220 $\text{m}^2 \text{g}^{-1}$ regardless of the pyrolysis temperature, due to the presence of residual carbon in the materials which stabilized their porous structure and prevented extensive sintering of MnO and Co crystallites. Furthermore, the same research group synthesized Co-Mn spinel oxide via oxidative treatment of fumarate precursors and the calcined samples had considerably smaller surface area than pyrolyzed ones in the range of 21–35 $\text{m}^2 \text{g}^{-1}$ [6–8]. Faure et al. synthesized $\text{Co}_x\text{Mn}_{3-x}\text{O}_4$ ($0 \leq x \leq 3$) by thermal decomposition of oxalate precursor and concluded that the oxides with $x < 0.9$ are amorphous, while for $x > 0.9$ all the nanomaterials had a cubic spinel structure. According to TEM and XRD results, the crystallite size ranged between 6 ($x = 1.6$) and 16 ($x = 3$) nm. Regarding textural properties, the BET surface area and the pore volume were the highest for $x = 2$ ($S_{\text{BET}} = 270 \text{ m}^2 \text{ g}^{-1}$, pore volume = $0.48 \text{ cm}^3 \text{ g}^{-1}$) whereas further increase of cobalt content was associated with a decrease of surface area and pore volume [39].

The structure and physicochemical characteristics of cobalt aluminate (CoAl_2O_4) nanomaterials were investigated by means of XRD, FTIR, TEM and SEM. Wang et al. synthesized $\text{Co}^{\text{II}}\text{Co}^{\text{III}}\text{Al}_{2-x}\text{O}_4$ ($x = 0-2$) and reported that nanomaterials had spinel cubic structure (Fd3m) and that their crystallite size ranged between 9 and 51 nm depending on Co/Al ratio and pyrolysis temperature. Their formation was further validated by FTIR spectroscopy from the appearance of the characteristic vibrational bands of CoAl_2O_4 (572 and 668 cm^{-1}). According to SEM images the spinel samples were agglomerated in large particles with irregular shape. The BET surface area was 22–69 $\text{m}^2 \text{g}^{-1}$ depending on annealing temperature [40]. Gingasu et al. investigated the physicochemical properties of CoCr_2O_4 nanomaterials synthesized by thermal decomposition of tartrate and gluconate precursors. The reflections of XRD patterns could be indexed to the face-centered cubic cell with the Fd3m space group and the average crystallite size obtained from tartrate and gluconate precursors was 14–18 and 21 nm, respectively. According to SEM and TEM micrographs, the particle size of CoCr_2O_4 obtained from tartrate was in the range 13–35 nm (depending on annealing temperature), while CoCr_2O_4 obtained from gluconate was in the range 16–28 nm showing in each case well-faceted pyramidal or bipyramidal geometry. CoCr_2O_4 from gluconate precursor formed spherical aggregates with an average size 200–400 nm. The formation of cobalt chromite nanomaterials was confirmed by the presence of sharp and intense bands in the range 615–640 and 500–530 cm^{-1} in FTIR spectra, which are characteristic of Cr-O bonds. According to Raman spectra, the spinel

type CoCr_2O_4 has a cubic symmetry where the Co^{2+} and Cr^{3+} ions occupy the tetrahedral and octahedral sites, respectively. Furthermore, the nitrogen adsorption isotherms were of IV type with a H3 hysteresis loop, characteristic for mesoporous materials. The BET surface area and pore parameters for tartrate-derived CoCr_2O_4 were $S_{\text{BET}} = 15\text{--}51 \text{ m}^2 \text{ g}^{-1}$, pore volume = $0.11\text{--}0.24 \text{ cm}^3 \text{ g}^{-1}$ and average pore diameter = $21\text{--}32 \text{ nm}$, whereas for gluconate-derived CoCr_2O_4 were $17\text{--}42 \text{ m}^2 \text{ g}^{-1}$, $0.15\text{--}0.21 \text{ cm}^3 \text{ g}^{-1}$ and $21\text{--}34 \text{ nm}$, respectively [41]. Darbar et al. synthesized MgCo_2O_4 by oxalate decomposition and XRD patterns were indexed to the standard cubic structure with Fd3m space group. The SEM images revealed the agglomeration of MgCo_2O_4 nanoparticles and the BET surface area was measured in the range $4\text{--}22 \text{ m}^2 \text{ g}^{-1}$ depending on calcination temperature [42]. Kim et al. produced NiCo_2O_4 aggregates by oxalate decomposition and the XRD pattern confirmed the formation of cubic spinel NiCo_2O_4 phase with minor additional impurities (NiO). SEM micrographs showed the presence of various morphologies, such as micro flowers and rod shapes and according to TEM images each microstructure consisted of aggregates of spherical metal-oxide nanoparticles with diameter between 20 and 100 nm [43]. Seyfi et al. reported on the synthesis of LaCoO_3 perovskite catalysts with specific surface area of $5 \text{ m}^2 \text{ g}^{-1}$ [44]. On the other hand, Gabal et al. produced purely trigonal ilmenite CoTiO_3 by thermal treatment of cobalt oxalate- TiO_2 precursor. They concluded that at high temperature (1000°C), CoTiO_3 with rhombohedral symmetry (space group R-3 (148)) was formed. According to TEM images, the nanomaterial showed weak agglomeration with heterogeneous morphology in both shape and dimensions and exhibited a larger grain size, 300 nm, compared to that estimated from Scherrer's equation, 209 nm, due to the agglomeration nature of the nanoparticles as observed from the TEM micrograph. In addition, the specific surface area of the sample was $30 \text{ m}^2 \text{ g}^{-1}$ and the adsorption isotherm was classified to type II, characteristic for macroporous adsorbents and had very small hysteresis loop [45].

6.5. Structure and characterization of supported cobalt oxide nanoparticles

The results from XRD analysis of cobalt compounds supported on carbonaceous carriers differ depending on the nature of the compound (Co_3O_4 , CoO , Co) but in all cases reflections corresponding to the lattice planes of graphitic materials have been observed. The reflections due to cobalt/cobalt oxide nanoparticles were similar to those mentioned above for unsupported materials or in some cases they were not detected at all. It is obvious that an increase in the carbon content leads to an increase of the graphitic diffraction peaks and simultaneous decrease of cobalt/cobalt oxide peaks. Additionally, with increasing calcination temperature, the diffraction peaks for cobalt/cobalt oxide became sharper in contrast to those for carbon, indicating that the crystallinity of cobalt-based nanoparticles increased and graphite content decreased due to its partial oxidation [47]. According to SEM and TEM micrographs, cobalt-based nanoparticles were spherical, coated with carbon and dispersed in the carbon matrix [54], uniformly distributed on carbon layered structures with particle size of $5\text{--}30 \text{ nm}$ [53], supported on carbon with random size distribution in the range from 1 to 32 nm [50], embedded in carbon with average particle size of $8\text{--}10 \text{ nm}$ [51] and encapsulated within carbon

nanotubes with an average particle size of 50 nm [52]. N₂ adsorption-desorption isotherms of the as-synthesized nanocomposites exhibited the type IV isotherm with a H3-type hysteresis loop, demonstrating the mesoporous nature of the materials, while the textural properties of the materials varied widely ($S_{\text{BET}} = 76\text{--}365 \text{ m}^2 \text{ g}^{-1}$, pore volume = $0.15\text{--}0.96 \text{ cm}^3 \text{ g}^{-1}$, average pore size = $1.5\text{--}20 \text{ nm}$) [50, 52–54]. However, Zhou et al. observed a N₂ adsorption isotherm of type V with a H3-type hysteresis loop, while the specific surface area ranged between 160 and $375 \text{ m}^2 \text{ g}^{-1}$, the pore volume was $0.58\text{--}0.98 \text{ cm}^3 \text{ g}^{-1}$ and the average pore size varied from 4.8 to 6.9 nm depending on the calcination temperature [51]. In many publications, electrical and magnetic properties have been investigated due to the potential use of the as-synthesized materials in Li-ion batteries and as electrocatalysts [47, 52–54].

7. Applications of cobalt-based nanoparticles

The structure and physicochemical characteristics of cobalt-based nanomaterials make them suitable candidates as catalysts for various processes, that is, alcohol reforming, Fischer-Tropsch, oxidation of organic compounds and CO, as oxygen electrocatalysts and as electrode materials in lithium-ion batteries.

There has been a significant effort to decrease the dependence on non-renewable fossil fuels and move toward sustainable energy carriers, such as hydrogen derived from renewable sources. H₂ is considered to be the energy carrier of the future and the use of liquid bio-fuels, such as ethanol and methanol, as hydrogen carriers is an attractive option. Thus, H₂ production from alcohol steam reforming has been of great interest and has been extensively investigated. Since alcohol reforming is a catalytic process, various catalytic systems have been tested aiming at optimization of their efficiency. Among them, cobalt-based catalysts are promising candidates. Papadopoulou et al. prepared Co-MnO catalysts by pyrolytic decomposition of the corresponding fumarate and gluconate salts and examined them in methanol and ethanol reforming. They concluded that catalysts with the highest cobalt loading were the most active both in methanol and ethanol reforming. The utilization of fumarate-derived Co-MnO catalysts led to complete methanol conversion at $375\text{--}400^\circ\text{C}$ (high-temperature methanol reforming compared to copper-based catalysts), while complete ethanol conversion was achieved at 480°C (low-temperature ethanol reforming compared to noble-metal catalysts). Thus, reforming of both alcohols took place under comparable conditions at temperatures in the range of $400\text{--}450^\circ\text{C}$. The advantages of the proposed method of catalyst preparation were the formation of the reduced active state of the catalysts in a single step and the existence of residual carbon, which hindered sintering and excessive particle growth under synthesis and reaction conditions [6–8]. Abdelkader et al. studied the catalytic activity of Co₃O₄, Fe₂O₃ and corresponding mixed Co-Fe in the steam reforming of ethanol and concluded that the mixed Co-Fe sample exhibited higher H₂ yield, greater selectivity to CO and CO₂ and reduced by-product formation compared to pure Co₃O₄, Fe₂O₃ and physical Co-Fe mixture [14].

Rechargeable lithium-ion batteries (LIBs) are the most utilized energy storage devices for portable electronics and one of the most promising electrode materials are cobalt-based nanomaterials in place of carbon. Novel porous Co_3O_4 architectures [18, 19], MgCo_2O_4 nanomaterials [42], Co_3O_4 /graphite composites [47], cobalt-based nanoparticles embedded in nitrogen-doped nanotubes [52] and carbon-coated Co_3O_4 nanoparticles [54] have been studied regarding their electrochemical performance. Briefly, Yuan et al. reported on the performance of Co_3O_4 polyhedral architectures and showed that they exhibited high discharge capacities for many discharge/charge cycles, due to their porous structure [18]. Yuan et al. synthesized nanosized Co_3O_4 and concluded that the advantage of this material over carbon was due to its higher capacity per unit volume (7.5 times in comparison to carbon) and that the particle size affected its electrochemical properties (the optimum average particle size was 37 nm) [19]. Guo et al. studied the electrochemical properties of Co_3O_4 /graphite composites and showed that the reversible capacity increased with decrease in graphite content and increase in the calcination temperature, while cycling stability decreased dramatically with decrease in graphitic content [47]. Khan et al. reported on the excellent performance of cobalt oxide nanoparticles embedded in nitrogen-doped carbon nanotubes, which is attributed to the nitrogen doping of carbon nanotubes, the strong interaction between the encapsulated cobalt oxide nanoparticles with the carbon nanotubes, the porosity and the specific surface area of the nanomaterial [52]. In addition, Qiu et al. investigated the electrochemical performance of carbon-coated Co_3O_4 nanoparticles in comparison to bare Co_3O_4 electrode and concluded that the superior electrode performance of the first was attributed to better dispersion and to the thin carbon shell coating of the nanoparticles on the electrode surface [54].

Lu et al. showed that the utilization of Co-MOFs for the fabrication of metallic Co nanoparticles embedded in nitrogen-doped porous carbon layers led to the production of an efficient electrocatalyst with bifunctional activities toward oxygen reduction and evolution reactions (ORR, OER) in alkaline media due to nitrogen doping and embedded cobalt nanoparticles in the carbon structure [53].

Concerning environmental catalysis, the strict environmental legislation for pollutant emissions and the high-cost of noble-metal catalysts has shifted interest toward the production of effective transition metal-oxide catalysts. Cobalt-based nanomaterials, such as nanocrystalline Co_3O_4 , Co-Ce composite oxide, CoFe_2O_4 and Co-Mn oxide spinels have been synthesized by thermal decomposition of organic precursors and studied in various pollutant abatement processes. de Rivas et al. have examined nanocrystalline Co_3O_4 catalysts in the gas-phase oxidation of chlorinated short chain alkanes and reported on their enhanced catalytic behavior as they exhibited high conversion to deep oxidation products (CO_2 , HCl , Cl_2) at low temperatures with excellent selectivity to CO_2 and resistance to deactivation [15, 20]. Similar experiments have been conducted by Wang et al. using Co-Ce catalysts [22]. Liu et al. have demonstrated the excellent activity and stability of Co_3O_4 -based catalysts for propane catalytic combustion [21]. Faure et al. synthesized Co-Mn-oxide spinel catalysts and concluded that their high activity for CO oxidation was correlated to both their surface area and cobalt concentration. Among the synthesized nanomaterials, $\text{Co}_{2.3}\text{Mn}_{0.7}\text{O}_4$ exhibited higher activity than cobalt oxide catalysts [39]. Co_3O_4 nanoparticles [48] and LaCoO_3 nano-perovskite [44] catalysts were also

investigated for CO oxidation reaction and exhibited good structural and chemical stability and high activity. Additionally, Ashouri et al. employed MOF-derived Co_3O_4 for the catalytic oxidation and epoxidation of olefins and reported that the catalyst showed good catalytic stability and reusability [49]. Diodati et al. synthesized and used CoFe_2O_4 in the catalytic oxidation of methane and concluded that the catalytic reaction took place at lower temperature (by about 300 K) in comparison to the uncatalyzed reaction while the cobalt ferrite catalyst exhibited good stability [30]. Gingasu et al. synthesized cobalt chromite catalysts via thermal decomposition of tartrate and gluconate precursors and reported that gluconate-derived CoCr_2O_4 was the best catalyst for total oxidation of methane exhibiting high activity and CO_2 selectivity [41]. Co nanoparticles embedded in mesoporous nitrogen-doped carbon were investigated by Zhou et al. for the reductive amination of carbonyl compounds with nitro compounds by transfer hydrogenation with formic acid and found them to be active and selective with excellent yields for secondary amines [51]. Another reported application of cobalt-based nanoparticles is in water treatment for the removal of dye pollutants. Advanced oxidation processes and especially Fenton reactions are considered to be among the most feasible pollutant degradation technologies [16, 55].

One of the most significant applications of cobalt nanomaterials in catalysis, is in Fischer-Tropsch synthesis. The Fischer-Tropsch process targets the production of synthetic liquid fuels using coal, natural gas and biomass and hydrogen derived from renewable electricity as feedstocks. Cobalt-based catalysts have been employed to a great extent since they have high selectivity for long chain hydrocarbons and low selectivity for the water-gas shift reaction and they are cost-effective. The reducibility, cobalt dispersion and loading and nanoparticle structure are some of the parameters that affect the catalytic activity and selectivity. Pei et al. synthesized fully reduced carbon-supported cobalt catalysts by pyrolysis of Co-MOF-71 precursor and showed that the as-prepared catalysts had extremely high Co site density, high activity and selectivity with diesel fuels being the main products and high C_{5+} space-time yields in comparison to conventional cobalt catalysts [50].

8. Conclusions

Nanostructured cobalt-based materials have attracted considerable interest due to their multiple applications in various fields, like catalysis, electronics, electrochemical devices, etc. Among the synthesized cobalt nanomaterials, Co_3O_4 is by far the main nanostructure been reported in the literature, whereas fewer studies have been made regarding CoO, metallic Co, mixed metal-oxide nanoparticles or other types of cobalt-based nanomaterials. A great number of methods have been employed for their synthesis with the thermal decomposition of organic precursors bearing noteworthy advantages as, for instance, simplicity, short processing time and cost-effectiveness. Carboxylate salts (e.g. oxalate, citrate, etc.) as well as metal-organic frameworks (MOFs) are utilized as organic precursors for the production of cobalt oxides, metallic cobalt, mixed cobalt oxides and

supported cobalt-based nanomaterials. The nature of organic precursor, the precursor synthesis method, the cobalt content, the combination with other elements, the treatment schedule and temperature and the type of the gaseous atmosphere (oxidizing, inert, reducing) prevailing during heating are some of the factors that affect the physical and chemical properties of the final composite. The relevant nanomaterials have been extensively characterized and analyzed using various techniques (XRD, FTIR, SEM, TEM, XPS, Raman, etc.) and accounts have been reported on their novel properties in comparison to bulk solids. A non-exhaustive list of potential applications of such cobalt-based nanomaterials includes catalysts for Fischer-Tropsch process, alcohol reforming, oxidation of organic compounds and CO, oxygen electrocatalysts and anode materials for Li-ion batteries.

Author details

Maria Smyrnioti^{1,2} and Theophilos Ioannides^{1*}

*Address all correspondence to: theo@iceht.forth.gr

1 Foundation for Research & Technology – Hellas, Institute of Chemical Engineering Sciences (FORTH/ICE-HT), Patras, Greece

2 Department of Chemistry, University of Patras, Greece

References

- [1] Thangavelu K, Parameswari K, Kuppusamy K, Haldorai Y. A simple and facile method to synthesize Co_3O_4 nanoparticles from metal benzoate dihydrazinate complex as a precursor. *Materials Letters*. 2011;**65**:1482-1484
- [2] Luisetto I, Pepe F, Bemporad E. Preparation and characterization of nano cobalt oxide. *Journal of Nanoparticle Research*. 2008;**10**:59-67
- [3] Stefanescu O, Davidescu C, Muntean C. Preparation and characterization of cobalt oxides nanoparticles starting from Co(II) carboxylate precursors. *Journal of Optoelectronics and Advanced Materials*. 2015;**17**:991-996
- [4] Thota S, Kumar A, Kumar J. Optical, electrical and magnetic properties of Co_3O_4 nanocrystallites obtained by thermal decomposition of sol-gel derived oxalates. *Materials Science and Engineering B*. 2009;**164**:30-37
- [5] Bartůněk V, Huber Š, Sedmidubský D, Sofer Z, Šimek P, Jankovský O. CoO and Co_3O_4 nanoparticles with a tunable particle size. *Ceramics International*. 2014;**40**:12591-12595
- [6] Papadopoulou E, Delimaris D, Denis A, Machocki A, Ioannides T. Alcohol reforming on cobalt-based catalysts prepared from organic salt precursors. *International Journal of Hydrogen Energy*. 2012;**37**:16375-16381

- [7] Papadopoulou E, Ioannides T. Methanol Reforming over Cobalt Catalysts Prepared from Fumarate Precursors: TPD Investigation. *Catalysts*. 2016;**6**:33
- [8] Papadopoulou E, Ioannides T. Steam reforming of methanol over cobalt catalysts: Effect of cobalt oxidation state. *International Journal of Hydrogen Energy*. 2015;**40**:5251-5255
- [9] Semenov SA, Drobot DV, Musatova VY, Pronin AS, Pomogailob AD, Dzhardimalieva GI, Popenko VI. Synthesis and thermal conversions of unsaturated cobalt(II)dicarboxylates as precursors of metallopolymer nanocomposites. *Russian Journal of Inorganic Chemistry*. 2015;**60**:897-905
- [10] Mohamed MA, Galwey AK, Halawy SA. Kinetic and thermodynamic study of the non-isothermal decompositions of cobalt malonate dihydrate and of cobalt hydrogen malonate dihydrate. *Thermochimica Acta*. 2000;**346**:91-103
- [11] Dippong T, Berinde Z, Pauliuc I. Formation and evolution of crystalline magnetic phases of CoFe_2O_4 with temperature depending on the nature of the diol used. *Journal of Magnetism and Magnetic Materials*. 2013;**334**:87-95
- [12] Manouchehri I, Kameli P, Salamati H. Facile Synthesis of $\text{Co}_3\text{O}_4/\text{CoO}$ Nanoparticles by thermal treatment of ball-milled precursors. *Journal of Superconductivity and Novel Magnetism*. 2011;**24**:1907-1910
- [13] Ganguly A, Kundu R, Ramanujachary KV, Lofland SE, Das D, Vasanthacharya NY, Ahmad T, Ganguli AK. Role of carboxylate ion and metal oxidation state on the morphology and magnetic properties of nanostructured metal carboxylates and their decomposition products. *Journal of Chemical Sciences*. 2008;**120**:521-528
- [14] Abdelkader A, Daly H, Saih Y, Morgan K, Mohamed MA, Halawy SA, Hardacre C. Steam reforming of ethanol over $\text{Co}_3\text{O}_4\text{-Fe}_2\text{O}_3$ mixed oxides. *International Journal of Hydrogen Energy*. 2013;**38**:8263-8275
- [15] de Rivas B, López-Fonseca R, Jiménez-González C, Gutiérrez-Ortiz JI. Highly active behaviour of nanocrystalline Co_3O_4 from oxalate nanorods in the oxidation of chlorinated short chain alkanes. *Chemical Engineering Journal*, 2012;**184**:184-192
- [16] Shen Y, Zhang Z, Xiao K. Evaluation of cobalt oxide, copper oxide and their solid solutions as heterogeneous catalysts for Fenton-degradation of dye pollutants. *RSC Advances*. 2015;**5**:91846-91854
- [17] Manteghi F, Kazemi SH, Peyvandipoor M, Asghari A. Preparation and application of cobalt oxide nanostructures as electrode materials for electrochemical supercapacitors. *RSC Advances*. 2015;**5**:76458-76463
- [18] Yuan W, Xie D, Dong Z, Su Q, Zhang J, Du G, Xu B. Preparation of porous Co_3O_4 polyhedral architectures and its application as anode material in lithium-ion battery. *Materials Letters*. 2013;**97**:129-132
- [19] Yuan Z, Huang F, Feng C, Sun J, Zhou Y. Synthesis and electrochemical performance of nanosized Co_3O_4 . *Materials Chemistry and Physics*. 2003;**79**:1-4

- [20] de Rivas B, López-Fonseca R, Jiménez-González C, Gutiérrez-Ortiz JI. Synthesis, characterisation and catalytic performance of nanocrystalline Co_3O_4 for gas-phase chlorinated VOC abatement. *Journal of Catalysis*. 2011;**281**:88-97
- [21] Liu Q, Wang L-C, Chen M, Cao Y, He H-Y, Fan K-N. Dry citrate-precursor synthesized nanocrystalline cobalt oxide as highly active catalyst for total oxidation of propane. *Journal of Catalysis*. 2009;**263**:104-113
- [22] Wang C, Zhang C, Hua W, Guo Y, Lu G, Gil S, Giroir-Fendler A. Catalytic oxidation of vinyl chloride emissions over Co-Ce composite oxide catalysts. *Chemical Engineering Journal*. 2017;**315**:392-402
- [23] Pudukudy M, Yaakob Z, Narayanan B, Gopalakrishnan A, Tasirin SM. Facile synthesis of bimodal mesoporous spinel Co_3O_4 nanomaterials and their structural properties. *Superlattices and Microstructures*. 2013;**64**:15-26
- [24] Stefanescu M, Dippong T, Stoia M, Stefanescu O. Study on the obtaining of cobalt oxides by thermal decomposition of some complex combinations, undispersed and dispersed in SiO_2 matrix. *Journal of Thermal Analysis and Calorimetry*. 2008;**94**:389-393
- [25] Bhattacharjee CR, Purkayastha DD, Das N. Surfactant-free thermal decomposition route to phase pure tricobalt tetraoxide nanoparticles from cobalt(II)-tartrate complex. *Journal of Sol-Gel Science and Technology*. 2013;**65**:96-300
- [26] Palacios-Hernández T, Hirata-Flores GA, Contreras-López OE, Mendoza-Sánchez ME, Valeriano-Arreola I, González-Vergara E, Méndez-Rojas MA. Synthesis of Cu and Co metal oxide nanoparticles from thermal decomposition of tartrate complexes. *Inorganica Chimica Acta*. 2012;**392**:277-282
- [27] Chen Z, Xu A, Yu Zhang NG. Preparation of NiO and CoO nanoparticles using M^{2+} -oleate (M = Ni, Co) as precursor. *Current Applied Physics*. 2010;**10**:967-970
- [28] Assim K, Schulze S, Pügner M, Uhlemann M, Gemming T, Giebeler L, Hietschold M, Lampke T, Lang H. Co(II) ethylene glycol carboxylates for Co_3O_4 nanoparticle and nanocomposite formation. *Journal of Materials Science*. 2017;**52**:6697-6711
- [29] Gawande MB, Pandeyb RK, Jayaram RV. Role of mixed metal oxides in catalysis science – versatile applications in organic synthesis. *Catalysis Science & Technology*. 2012;**2**:1113-1125
- [30] Diodati S, Nodari L, Natile MM, Caneschi A, de Julián Fernández C, Hoffmann C, Kaskel S, Lieb A, Di Noto V, Mascoto S, Saini R, Gross S. Coprecipitation of oxalates: An easy and reproducible wet-chemistry synthesis route for transition-metal ferrites. *European Journal of Inorganic Chemistry*. 2014;**5**:875-887
- [31] Dippong T, Levei EA, Cadar O. Preparation of $\text{CoFe}_2\text{O}_4/\text{SiO}_2$ nanocomposites at low temperatures using short chain diols. *Journal of Chemistry, Hindawi*. 2017;**2017**:Article ID: 7943164

- [32] Stefanescu M, Stoia M, Caizer C, Dippong T, Barvinschi P. Preparation of $\text{Co}_x\text{Fe}_{3-x}\text{O}_4$ nanoparticles by thermal decomposition of some organo-metallic precursors. *Journal of Thermal Analysis and Calorimetry*. 2009;**97**:245-250
- [33] Barvinschi P, Stefanescu O, Dippong T, Sorescu S, Stefanescu M. $\text{CoFe}_2\text{O}_4/\text{SiO}_2$ nanocomposites by thermal decomposition of some complex combinations embedded in hybrid silica gels. *Journal of Thermal Analysis and Calorimetry*. 2013;**112**:447-453
- [34] Dippong T, Levei EA, Cadar O, Mesaros A, Borodi G. Sol-gel synthesis of $\text{CoFe}_2\text{O}_4:\text{SiO}_2$ nanocomposites – insights into the thermal decomposition process of precursors. *Journal of Analytical and Applied Pyrolysis*. 2017;**125**:169-177
- [35] Dippong T, Levei EA, Cadar O, Goga F, Borodi G, Barbu-Tudoran L. Thermal behavior of $\text{Co}_x\text{Fe}_{3-x}\text{O}_4/\text{SiO}_2$ nanocomposites obtained by a modified sol-gel method. *Journal of Thermal Analysis and Calorimetry*. 2017;**128**:39-52
- [36] Amiri M, Niasari MS, Akbari A, Razavi R. Sol-gel auto-combustion synthesis and characterization of a novel anticorrosive cobalt ferrite nanoparticles dispersed in silica matrix. *Journal of Materials Science: Materials in Electronics*. 2017;**28**:10495-10508
- [37] Muntean C, Bozdog M, Duma S, Stefanescu M. Study on the formation of $\text{Co}_{1-x}\text{Zn}_x\text{Fe}_2\text{O}_4$ system using two low-temperature synthesis methods. *Journal of Thermal Analysis and Calorimetry*. 2016;**123**:117-126
- [38] Stefanescu M, Bozdog M, Muntean C, Stefanescu O, Vlase T. Synthesis and magnetic properties of $\text{Co}_{1-x}\text{Zn}_x\text{Fe}_2\text{O}_4$ ($x = 0-1$) nanopowders by thermal decomposition of Co(II) , Zn(II) and Fe(III) carboxylates. *Journal of Magnetism and Magnetic Materials*. 2015;**393**:92-98
- [39] Faure B, Alphonse P. Co–Mn-oxide spinel catalysts for CO and propane oxidation at mild temperature. *Applied Catalysis. B, Environmental*. 2016;**180**:715-725
- [40] Wang C, Liu S, Liu L, Bai X. Synthesis of cobalt-aluminate spinels via glycine chelated precursors. *Materials Chemistry and Physics*. 2006;**96**:361-370
- [41] Gingasu D, Mindru I, Culita DC, Patron L, Calderon-Moreno JM, Osiceanu P, Preda S, Oprea O, Parvulescu V, Teodorescu V, Walsh JPS. Structural, magnetic and catalytic properties of cobalt chromite obtained through precursor method. *Materials Research Bulletin*. 2015;**62**:52-64
- [42] Darbar D, Reddy MV, Sundarajan S, Patabiraman R, Ramakrishna S, Chowdari BVR. Anodic electrochemical performances of MgCo_2O_4 synthesized by oxalate decomposition method and electrospinning technique for Li-ion battery application. *Materials Research Bulletin*. 2016;**73**:369-376
- [43] Kim BC, Rajesh M, Jang HS, Yu KH, Kim SJ, Park SY, Raj CJ. Facile synthesis and capacitive properties of nickel-cobalt binary metal oxide nanoaggregates via oxalate route. *Journal of Alloys and Compounds*. 2016;**674**:376-383

- [44] Seyfi B, Baghalha M, Kazemian H. Modified LaCoO_3 nano- perovskite catalysts for the environmental application of automotive CO oxidation. *Chemical Engineering Journal*. 2009;**148**:306-311
- [45] Gabal MA, Hameed SA, Obaid AY. CoTiO_3 via cobalt oxalate– TiO_2 precursor. Synthesis and characterization. *Materials Characterization*. 2012;**71**:87-94
- [46] Zhou H, Kitagawa S. Metal-Organic Frameworks (MOFs). *Chemical Society Reviews*. 2014;**43**:5415
- [47] Guo H, Li X, Li XH, Wang Z-X, Peng W, Sun Q, Xie J. Preparation and electrochemical properties of Co_3O_4 /graphite composites as anodes of lithium ion batteries. *Journal of Central South University of Technology*. 2010;**17**:498-503
- [48] Wang W, Li Y, Zhang R, He D, Liu H, Liao S. Metal-organic framework as a host for synthesis of nanoscale Co_3O_4 as an active catalyst for CO oxidation. *Catalysis Communications*. 2011;**12**:875-879
- [49] Ashouri F, Zare M, Bagherzadeh M. Manganese and cobalt-terephthalate metal-organic frameworks as a precursor for synthesis of Mn_2O_3 , Mn_3O_4 and Co_3O_4 nanoparticles: Active catalysts for olefin heterogeneous oxidation. *Inorganic Chemistry Communications*. 2015;**61**:73-76
- [50] Pei Y, Li Z, Li Y. Highly Active and Selective Co-Based Fischer-Tropsch Catalysts Derived from Metal–Organic Frameworks. *AICHE Journal*. 2017;**63**(7):2935-2944
- [51] Zhou P, Zhang Z, Jiang L, Yu C, Lv K, Sun J, Wang S. A versatile cobalt catalyst for the reductive amination of carbonyl compounds with nitro compounds by transfer hydrogenation. *Applied Catalysis. B, Environmental*. 2017;**210**:522-5329
- [52] Khan IA, Nasim F, Choucair M, Ullah S, Badshah A, Nadeem MA. Cobalt oxide nanoparticles embedded N-CNTs: Lithium ion battery applications. *RSC Advances*. 2016;**6**(2):1129-1135
- [53] Lu H, Zhang H, Liu R, Zhang X, Zhao H, Wang G. Macroscale cobalt-MOFs derived metallic Co nanoparticles embedded in N-doped porous carbon layers as efficient oxygen electrocatalysts. *Applied Surface Science*. 2017;**392**:402-409
- [54] Qiu B, Guo W, Liang Z, Xia W, Gao S, Wang Q, Yu X, Zhao R, Zou R. Fabrication of Co_3O_4 nanoparticles in thin porous carbon shells from metal-organic frameworks for enhanced electrochemical performance. *RSC Advances*. 2017;**7**:13340-13346
- [55] Huang Q, Zhang J, He Z, Shi P, Qin X, Yao W. Direct fabrication of lamellar self-supporting Co_3O_4 /N/C peroxydisulfate activation catalysts for effective aniline degradation. *Chemical Engineering Journal*. 2017;**313**:1088-1098
- [56] Dippong T, Levei EA, Borodi G, Goga F, Tudoran LB. Influence of Co/Fe ratio on the oxide phases in nanoparticles of $\text{Co}_x\text{Fe}_{3-x}\text{O}_4$. *Journal of Thermal Analysis and Calorimetry*. 2015;**119**:1001-1009

